



Article

Temporal Variation in Tower-Based Solar-Induced Chlorophyll Fluorescence and Its Environmental Response in a Chinese Cork Oak Plantation

Meijun Hu ^{1,2,3} , Xiangfen Cheng ^{1,2,3}, Jinsong Zhang ^{1,2,3,*}, Hui Huang ^{1,2,3}, Yu Zhou ^{1,2,3}, Xin Wang ^{1,2,3}, Qingmei Pan ^{1,2,3} and Chongfan Guan ^{1,2,3}

¹ Key Laboratory of Tree Breeding and Cultivation, National Forestry and Grassland Administration, Research Institute of Forestry, Chinese Academy of Forestry, Beijing 100091, China; lkyhumj@caf.ac.cn (M.H.); chengxf@caf.ac.cn (X.C.); huanghui@caf.ac.cn (H.H.); zhouyucaf@caf.ac.cn (Y.Z.); wangxin@caf.ac.cn (X.W.); pqmei@caf.ac.cn (Q.P.); cagfcf123@caf.ac.cn (C.G.)

² Collaborative Innovation Center of Sustainable Forestry in Southern China, Nanjing Forest University, Nanjing 210037, China

³ Henan Xiaolangdi Earth Critical Zone National Research Station on the Middle Yellow River, Jiyuan 454650, China

* Correspondence: zhangjs@caf.ac.cn

Abstract: With the development of spectrum observation technology, solar-induced chlorophyll fluorescence (SIF)—an effective substitute for photosynthesis—has been widely used to monitor crop stress, vegetation phenology and ecosystem productivity. The relationship between fluorescence and photosynthesis is complicated because they are sensitive to environmental changes. Understanding the response of SIF to environmental factors is of great significance for clarifying the variation dynamic and relationship between SIF and photosynthesis under different conditions. In this study, the canopy SIF and the environmental factors of a *Quercus variabilis* BI. plantation were observed simultaneously, and the response of SIF to environmental factors at a daily scale and at a half-hour scale was analyzed. The results showed that SIF had obvious seasonal and diurnal dynamics and was mainly driven by photosynthetically active radiation (PAR). The influence of PAR, air temperature (Ta), vapor pressure deficit (VPD), soil moisture (SM) and wind speed (Ws) on SIF varied with the lapse of the growing season. After eliminating the covariant effect of PAR on the Ta and VPD during the whole growing season, the relationship between VPD and SIF was found to be negative, and the effect of Ta on SIF disappeared. This study enriched the ground observation dataset and provided support for understanding the variations in the relationship between SIF and photosynthesis under different conditions.

Keywords: SIF; temporal dynamic; tower-based observation; *Quercus variabilis* BI. plantation; environmental factors



Citation: Hu, M.; Cheng, X.; Zhang, J.; Huang, H.; Zhou, Y.; Wang, X.; Pan, Q.; Guan, C. Temporal Variation in Tower-Based Solar-Induced Chlorophyll Fluorescence and Its Environmental Response in a Chinese Cork Oak Plantation. *Remote Sens.* **2023**, *15*, 3568. <https://doi.org/10.3390/rs15143568>

Academic Editor: Liming He

Received: 1 June 2023

Revised: 12 July 2023

Accepted: 14 July 2023

Published: 16 July 2023



Copyright: © 2023 by the authors. Licensee MDPI, Basel, Switzerland. This article is an open access article distributed under the terms and conditions of the Creative Commons Attribution (CC BY) license (<https://creativecommons.org/licenses/by/4.0/>).

1. Introduction

As the most widely distributed producer in terrestrial ecosystems, plants participate in the carbon cycle by converting light energy into chemical energy through photosynthesis. In the context of global climate change, extreme climate events occur frequently [1], which may lead to the degradation of ecosystems and the loss of service functions [2]. Vegetation gross primary productivity (GPP) plays an important role in the global ecosystem's carbon cycle and can judge the production capacity of vegetation. GPP is affected by climate change and vegetation activity has feedback on the climate [3–5]. The main remote sensing models currently used to achieve estimations of the GPP at regional and global levels include the light use efficiency model [6], the photosynthetic mechanism process model [7] and the vegetation index model [8,9]. Among them, the vegetation index model has been widely used and developed because of its few input parameters and simple structure.

With the development of spectral observation techniques, researchers have found that solar-induced chlorophyll fluorescence (SIF) can capture the photosynthetic physiological information of plants quickly and non-destructively [10]. Compared with the conventional vegetation indices, which are based on canopy structure or vegetation greenness—such as the normalized difference vegetation index (NDVI), the enhanced vegetation index (EVI) and the leaf area index (LAI)—SIF, as a by-product of light reaction in plant photosynthesis, is more sensitive to physiological changes in the vegetation canopy [11]; therefore, it has been widely used in stress monitoring, phenology change and GPP estimations [12–15].

In recent years, SIF data have mainly come from satellite remote sensing [16,17], in situ observation [18,19] and unmanned aerial vehicle (UAV) systems [20,21]. The instantaneous value collected by the satellite or UAV lacks the ability to analyze the temporal dynamics of SIF. The pixels identified by satellite sensors usually cover a large area, and the data are usually mixed with information from multiple species, which will lead to divergence of SIF and GPP [22]. The accumulation of data under different spatio-temporal resolutions can clarify the characteristics of SIF, which is crucial in improving data availability. The tower-based fluorescence observation system usually has a high spectral resolution and signal-to-noise ratio, and can realize the continuous observation of the red and near-infrared wavelengths of canopy scale SIF, which is the main data source for current research studies on ground SIF [23–25]. Ground-based data provide important validation data for the development of optical fluorescence models and the validation of satellite products. Liu et al. established a GPP estimation mechanism model, driven by 760 nm canopy SIF, air temperature (T_a), photosynthetically active radiation (PAR) and other parameters [26]. The estimation results of this model showed higher accuracy compared with the observed GPP of winter wheat. Qiu et al. used ground SIF data to verify the improved model, BEPS-SIF, which was based on the boreal ecosystem productivity simulator. They applied the model to simulate and analyze SIF on a global scale [27]. Continuous canopy observations can clarify the change dynamics of SIF at different temporal scales and can have a better spatio-temporal identity with the ground data at ecosystem scales (such as the GPP and meteorological variables). This can provide a detailed and profound analysis of the coupling mechanism between fluorescence and photosynthesis [28].

The light energy absorbed by plant chlorophyll is released through a photochemical reaction, heat dissipation and fluorescence, which are all closely related to each other [29]. Environmental conditions will affect the proportion of the three pathways of energy dissipation after light absorption, which may change the emission of SIF [10]. According to the analysis of environmental factors and SIF in the Greater Khingan Mountains, the satellite SIF of 16 and 8 days was only correlated with the air temperature [30]. The tower-based SIF of evergreen forests was mainly affected by the half-hour PAR and soil moisture, while, at the daily scale, SIF was mainly regulated by air temperature [31]. Leaf fluorescence and non-photochemical quenching (NPQ) in maize and *Miscanthus* were correlated with both PAR and the leaf temperature [32]. SIF at different temporal and spatial scales has different responses to environmental factors. Environmental factors not only affect the fluorescent light energy utilization, but they also indirectly affect SIF by affecting stomatal conductance. Stomata are gas exchange channels between plants and the atmosphere, and the water status will affect the opening and closing of stomata. Stomatal conductance can determine the rate of gas exchange [33] and can influence radiation-use efficiency [34], which, in turn, affects photosynthesis and fluorescence light-use efficiency. Liu et al. found that soil moisture deficiency and a high vapor pressure deficit (VPD) changed the dynamics and intensity of SIF, and even changed the relationship between SIF and photosynthetic physiology [35]. Therefore, understanding the dynamics of SIF in different weather conditions and different temporal scales, and analyzing the response of SIF to environmental factors, are of great significance in accounting for the relationship between photosynthesis and fluorescence.

The dynamic change in SIF contains photosynthetic information, which is influenced by biological factors, abiotic factors, the canopy structure, the physiological state and other factors [36]. Due to differences in the fluorescence emission capacity and the canopy

structure, different types of vegetation usually have different dynamics and intensities [37]. Rossini et al. found that the fluorescence emission was the highest in farmland, followed by broadleaf forests, and was the lowest in coniferous forests [38]. The leaf fluorescence yield was found to be determined by genotype and to be affected by shading [39] and nitrogen availability [40]. The differences among species in terms of their carbon fixation pathways were more significant [22]. It was found that a canopy with a similar fraction of PAR could emit SIF in different intensities [41]. Due to the differences in the phenological characteristics and the photosynthetic physiology, the seasonal and diurnal dynamics of SIF were different among the species [42–44]. Moreover, the fluorescence was collected at the top of the canopy after it was emitted from the leaves and then absorbed and reabsorbed through the canopy [45,46]. For example, cropland ecosystems usually have a special row structure, and the observation angle will cause a variation in SIF [47]. Due to the special cluster structure of the leaves of coniferous forests, the light absorption capacity of the canopies in coniferous forests is higher than that in broadleaf forests [48]. Canopy structures, such as LAI and the leaf angle, not only determine the multiple scattering and absorption of radiation and fluorescence, they also affect the zenith and the azimuth angle [49]. According to previous studies on ecosystem water and the carbon flux constraints based on SIF, the simpler the canopy structure of vegetation, the higher the accuracy of the simulated value [50,51]. The canopies with complex structures are more likely to be affected by the sunlight observation geometry [52]. Although the application of SIF on a global scale has been recognized [14], the variability of SIF among species remains unsolved [53]. To date, there have been many species-specific SIF observations and studies on croplands; however, there have been few studies on forests, especially for deciduous broad-leaved forests, with obvious canopy structures and physiological variations.

In this study, the canopy SIF and the ecosystem's environmental factors in a *Quercus variabilis* Bl. (Chinese cork oak) plantation at the southern foot of Taihang Mountain were observed simultaneously. The response of the canopy SIF to the environmental factors was analyzed. This study was conducted to solve the following problems: (1) the dynamic characteristics of canopy SIF at different time scales; (2) the relationships between environmental factors and canopy SIF in different seasons and the response mechanism of SIF to environmental factors.

2. Materials and Methods

2.1. Study Site

We analyzed the 2020 warm–temperate, mixed forest ecosystem data from the national positioning observation and research station at the Henan Xiaolangdi Earth Critical Zone National Research Station on the Middle Yellow River (35°01'45"N, 112°28'08"E). The site is composed of Chinese cork oak, arborvitae (*Platycladus orientalis* L.) and locust (*Robinia pseudoacacia* L.), with Chinese cork oak accounting for more than 80%. The forest's age at the time the data were collected was 47 years, the average plant height was 8 m and the stand density was 998 trees/hm². Understory shrubs were dominated by *Grewia biloba* G. and *Vitex negundo* L., with thick litter layer and less herbs. The soil composition was mainly brown soil and limestone-weathered parent-material-leaching brown soil. The soil structure was poor: soil gravel content was high and the average soil depth was 50 cm. The station is located in Jiyuan City, Henan Province, in the Taihang Mountains, in the middle reaches of the Yellow River Basin, at an altitude of 410 m. It has a typical temperate monsoon climate, with a hot and rainy period. The average precipitation between June and September is 438.0 mm, accounting for 68.3% of the annual precipitation. The average annual temperature is 12.4 °C, the annual sunshine duration is 2367.7 h, the average annual precipitation is 641.7 mm, the annual evaporation is 1400 mm and the frost-free period is 220–230 days.

2.2. Data Acquisition

2.2.1. Observation of Environmental Factors

An automatic microclimate observation system was set up near the experimental site to continuously observe common parameters. T_a and relative humidity (RH) were recorded using temperature/humidity probes (HMP155, Vaisala Inc., Vantaa, Finland). The total radiation referred to the downward short-wave radiation was measured using a radiation transducer (CNR-4, Kipp & Zonen Inc., Delft, The Netherlands). PAR was recorded using photosynthetic photon sensor (LI-190SB, LI-COR Inc., Lincoln, NE, USA). Wind speed (W_s) was measured using an ultrasonic anemometer (Gill Windsonic, Gill Inc., Hampshire, UK). Soil moisture (SM) was measured using time-domain reflectometry (CS650, Campbell Scientific Inc., Logan, UT, USA). Precipitation was measured using a rainfall recorder (TE525MM, TEXAS ELECTRONICS Inc., Dallas, TX, USA). All environmental data were collected every minute and the 10 min average was recorded in the datalogger (CR1000, Campbell Scientific Inc., Logan, UT, USA). VPD refers to the difference between the saturated vapor pressure and the actual vapor pressure in the air at a certain temperature [54]. Daily environmental factors values were calculated as the mean of the observations between 6:00 and 19:30. The VPD was calculated as follows:

$$\text{VPD} = (1 - \text{RH}) \times 0.611 \times e^{\frac{17.27 \times T_a}{237.3 + T_a}} \quad (1)$$

2.2.2. Observation of Tower-Based Solar-Induced Chlorophyll Fluorescence

The automatic spectral observation system AUTOSIF-1 (Bergsun Inc., Beijing, China) was set up on the base platform, 10 m above the canopy of the closed forest, and the optical fibers were 5–6 m away from the tower. The observation system uses a QE65Pro spectrometer, with a spectral resolution of 0.31 nm, a sampling interval of 0.155 nm and a spectral range of 650–850 nm. The system is equipped with two optical fibers, in which the vertically up-facing fiber, with CC-3 cosine corrector (Ocean Optics Inc., Dunedin, FL, USA), was used to capture the downward solar irradiance, and the vertically down-facing bare fiber (field of view, 25°) was used to measure the upward radiance reflected from the canopy. The spectral automatic observation system measured the spectral data of descending irradiance and ascending radiance for approximately 3 min. The time interval between the measurement of irradiance spectrum and radiance spectrum was less than 10 s. The spectral fitting method (SFM) algorithm was built into the system to calculate the SIF value [55], and the reflectance of the canopy was continuously monitored during the growing season of Chinese cork oak—between March and November. Daily SIF were calculated as the mean of the observations between 6:00 and 19:30. The instrument was calibrated regularly and the original data were radiometrically calibrated before analysis. Due to the transmission path of radiation in the atmosphere in this study is short, we only carried out radiometric calibration and did not consider atmospheric correction [56].

2.3. Data Collation and Analysis

Vegetation indices can be used to reflect canopy structure, pigment and physiological changes, and can be retrieved by vegetation reflectance at specific wavelengths [57]. To confirm the research time range, we selected NDVI as a reference to judge the start and end time of the growing season of Chinese cork oak in 2020. Pigment affects the photosynthetic activity of vegetation, and the MERIS terrestrial chlorophyll index (MTCI) can reflect the canopy chlorophyll content. The calculation equation of NDVI [58] and MTCI [59,60] is as follows:

$$\text{NDVI} = \frac{R_{\text{NIR}} - R_{\text{red}}}{R_{\text{NIR}} + R_{\text{red}}} \quad (2)$$

$$\text{MTCI} = \frac{R_{\text{NIR}} - R_{\text{rededge}}}{R_{\text{rededge}} - R_{\text{red}}} \quad (3)$$

where R_{NIR} is the near-infrared reflectance range from 770 to 780 nm; R_{red} is the red reflectance range from 650 to 660 nm; and R_{rededge} is the red edge reflectance range from 700 to 710 nm. We determined the time of reaching the extremum of the first derivative of NDVI as the beginning and end of the growing season.

SIF is emitted by leaves after plants absorb light energy; it goes through the process of reabsorption in the canopy and then is finally observed at the top of canopy. Therefore, SIF is determined by absorbed photosynthetic active radiation (APAR), the SIF emission yield from all leaves in the canopy (ϕF) and fluorescence escape ratio (f_{esc}), as follows:

$$\text{SIF} = \text{APAR} \times \phi F \times f_{\text{esc}} \quad (4)$$

APAR is determined by the fraction of photosynthetically active radiation (fPAR), which is regulated by canopy structure and physiology. Since the red edge normalized difference vegetation index ($\text{NDVI}_{\text{rededge}}$) can characterize canopy structure and pigment changes [61], it has also been applied to the retrieval of fPAR. The calculation equation of APAR is as follows [62,63]:

$$\text{APAR} = \text{PAR} \times \text{fPAR} \quad (5)$$

$$\text{fPAR} = 1.37 \times \text{NDVI}_{\text{rededge}} - 0.17 \quad (6)$$

$$\text{NDVI}_{\text{rededge}} = \frac{R_{\text{NIR}} - R_{\text{rededge}}}{R_{\text{NIR}} + R_{\text{rededge}}} \quad (7)$$

According to the recent research, f_{esc} can be represented by near-infrared reflectance of vegetation (NIR_V) and fPAR [41,64], as follows:

$$f_{\text{esc}} \approx \frac{\text{NIR}_V}{\text{fPAR}} \quad (8)$$

$$\text{NIR}_V = \text{NDVI} \times R_{\text{NIR}} \quad (9)$$

According to the above equations, it follows that ϕF can be expressed as follows:

$$\phi F \approx \frac{\text{SIF}}{\text{PAR} \times \text{NIR}_V} \quad (10)$$

Weather had an impact on the analysis. We chose the clearness index (CI) [65,66] to represent the weather conditions (sunny or cloudy), and the calculation method was as follows:

$$\text{CI} = \frac{R_g}{R_0} \quad (11)$$

$$R_0 = S_0 \times \left[1 + 0.033 \times \cos\left(\frac{2\pi \times \text{DOY}}{365}\right) \right] \times \cos \theta \quad (12)$$

where R_g is the total solar radiation; R_0 is the extraterrestrial radiation at the top of the atmosphere; S_0 is the solar constant, denoted as $1367 \text{ W} \cdot \text{m}^{-2}$; and θ is the solar zenith angle. In previous research, 0.5 was usually chosen as the critical value to divide sunny (daily $\text{CI} > 0.5$) and cloudy (daily $\text{CI} \leq 0.5$) days [67]. The daily values of the parameters in this section were calculated as the mean of the observations between 6:00 and 19:30.

3. Results

3.1. Dynamics of Environmental Factors during Growing Season

To analyze the seasonal dynamics of SIF and the environmental factors of Chinese cork oak during the growing season, the NDVI was selected as a basis for identifying the growing season. The NDVI has an obvious seasonal variation in deciduous forests, which

can suggest the vegetation canopy greenness and growth. To discern the growing season of the forest, we chose the extreme value of the slope of the NDVI as the start (DOY = 81) and end time (DOY = 312) of the growing season. The seasonal dynamics of the NDVI in 2020 (Figure 1) revealed that the NDVI would increase first and then decrease, and the hill value was 0.93 (DOY = 126). The NDVI rose sharply, and the greenness increased during the sprouting and leaf unfolding in the spring. At the canopy closure, the NDVI reached its peak and remained in a relatively stable state. The NDVI decreased slowly at the end of the growth period and then rapidly during the defoliation period. It reached stability after defoliation. However, the decrease rate of the NDVI in the autumn was lower than the increase rate in the early growth stage. The MTCI and NDVI have similar seasonal trends. The difference was that the chlorophyll content increased sharply after the canopy leaf expansion and the NDVI increased sharply, reaching its maximum value of 8.78 (DOY = 142) in the spring. The MTCI decreased earlier than the NDVI, that is, the physiological senescence and the chlorophyll content decreased despite there being no significant change in the vegetation greenness. Overall, PAR and Ta showed a trend of first increasing and then decreasing, in the range 5.78–1367.85 $\mu\text{mol}\cdot\text{m}^{-2}\cdot\text{s}^{-1}$ and -7.6 – 32.3 °C, respectively. SM showed no obvious daily variation trend within the season, only increasing in different degrees after the occurrence of precipitation events, ranging from 10.6–20.6%. The dynamic of VPD in the growing season had no significant regularity, which was determined by the seasonal Ta and the unseasonal RH. Less precipitation in the spring and autumn can lead to a high VPD, which can easily cause meteorological drought events. However, more precipitation in the summer can lead to a smaller VPD. Overall, the seasonal mean value of the VPD in the growing season was spring (1.55 kPa) > autumn (1.21 kPa) > summer (1.14 kPa).

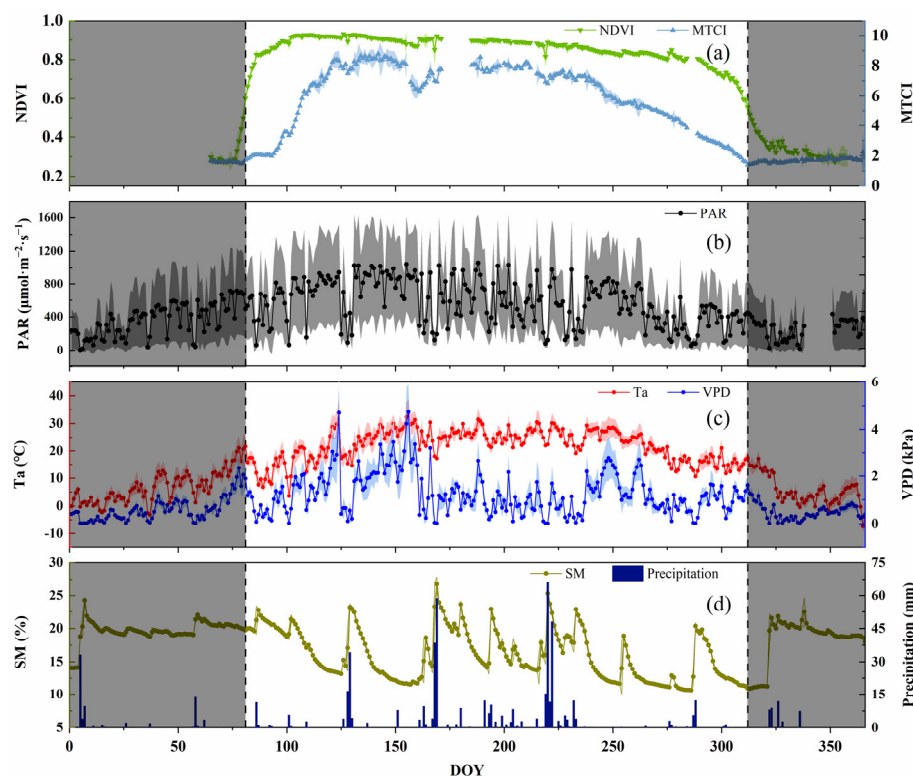


Figure 1. Seasonal dynamics of normalized difference vegetation index (NDVI); MERIS terrestrial chlorophyll index (MTCI); and environmental variables (photosynthetically active radiation—PAR; air temperature—Ta; vapor pressure deficit—VPD; soil moisture—SM; and precipitation) of Chinese cork oak plantation in 2020 ((a): NDVI and MTCI; (b): PAR; (c): Ta and VPD; (d): SM and precipitation). The points are the daily mean of the observations between 6:00 and 19:30. The shadows on either side of the point are the range of the standard deviations of the value. The shaded areas on both sides of the axis show the non-growing season.

3.2. Seasonal and Diurnal Dynamics of SIF

Just as the vegetation index represented the greenness and chlorophyll content, SIF showed an overall trend of first increasing and then decreasing in the growing season, with a range of $0.0225\text{--}0.8715\text{ mW}\cdot\text{m}^{-2}\cdot\text{sr}^{-1}\cdot\text{nm}^{-1}$. Moreover, the maximum value appeared at DOY = 115, which was earlier than the NDVI and MTCI (Figure 2). The seasonal dynamic of SIF showed acute fluctuations, with unapparent daily variation characteristics, which are easily affected by environmental factors, especially PAR. As a part of the SIF retrieval, the seasonal dynamics of APAR and SIF were consistent. fPAR determined APAR, and its trend was similar to the NDVI and MTCI, i.e., a combination of the two features. In other words, it was affected by the canopy structure and the chlorophyll content (Figure 1). The seasonal dynamics of the f_{esc} were opposite to those of the NDVI and MTCI.

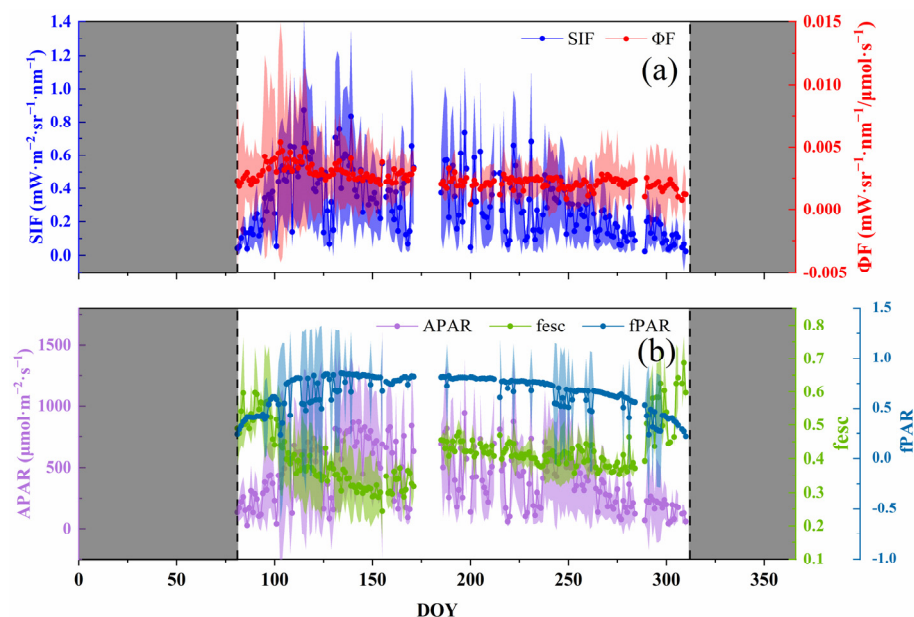


Figure 2. Seasonal dynamics of solar-induced chlorophyll fluorescence (SIF) and intermediate variables (absorbed photosynthetic active radiation, APAR; the fraction of emitted SIF that escapes from the canopy, f_{esc} ; the fraction of photosynthetically active radiation, fPAR; fluorescence emission yield, ΦF) ((a): SIF and ΦF); (b): APAR, f_{esc} and fPAR). The shadows on either side of the point are the range of standard deviations of the value. The shaded area on both sides of the axis is the non-growing season.

SIF is the energy released by vegetation after absorbing photosynthetically active radiation; therefore, it is affected by canopy structure, the vegetation's physiological situation and the environmental conditions. Environmental factors, especially PAR, affected SIF, which showed a violent fluctuation in 2020, without an obvious day-by-day pattern. To reveal the diurnal dynamics of SIF in different seasons under different weather conditions, we selected 3 contemporaneous days in each season, which were sunny, cloudy and rainy days, respectively. The results showed that SIF and PAR had relatively consistent diurnal variation under different weather conditions and seasons (Figure 3). SIF showed a single-peak curve on the sunny days; however, the SIF value fluctuated greatly on cloudy and rainy days, and its trend was basically consistent with PAR. The extent of the SIF value was driven by PAR, and its dynamic was earlier than PAR. In general, the SIF in the autumn was lower than that in the spring and summer, under all weather conditions. Under sunny conditions, the peak value of SIF appeared at 13:00 (spring), 12:30 (summer) and 11:30 (autumn), while the peak value of PAR in different seasons appeared at 13:00. With the progress of the growing season, the peak value of SIF gradually advanced. On cloudy days and rainy days, the time difference in the peak SIF and PAR was the same (both half an hour), and there was no change during the different seasons. To further analyze the

reasons for the difference of SIF during the different seasons and weather conditions, we analyzed the diurnal variation characteristics of APAR, ϕF and the f_{esc} in our calculation of SIF. ϕF was generally high in the morning, followed by a gradual decline with significant fluctuations (Figure 4). On sunny days, the diurnal dynamics of the f_{esc} were more severe, and, generally, in the afternoon, they were higher than in the morning. The fluctuation range of the intra-day f_{esc} in the spring was greater than that in the summer and autumn. The APAR diurnal dynamics were the same as SIF, but the rate of decline was higher in the afternoon, which may have been related to the higher f_{esc} .

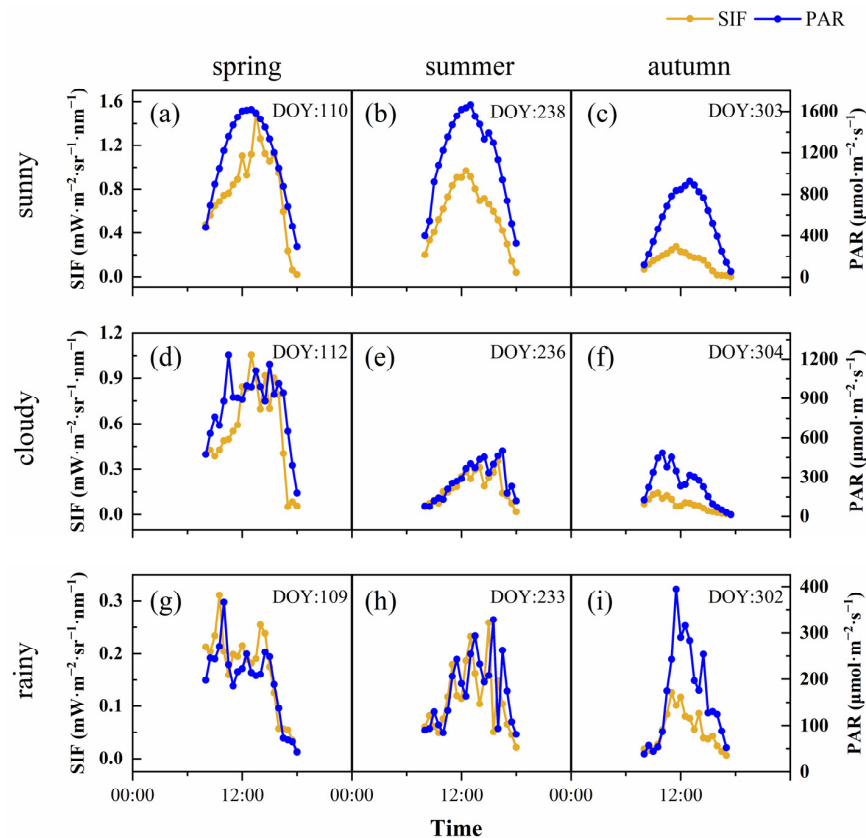


Figure 3. Diurnal dynamics of SIF (yellow line) and PAR (blue line) in spring (sunny (a), cloudy (d) and rainy (g)); summer (sunny (b), cloudy (e) and rainy (h)); and autumn (sunny (c), cloudy (f) and rainy (i)).

3.3. Correlation Analysis between SIF and Environmental Factors in Growing Season

Environmental factors can affect SIF by affecting the amount of light energy absorbed by leaves or the allocation of the light energy by the chlorophyll molecules. To clarify the similarities and differences in the SIF responses to the environmental factors in the different seasons, five factors were selected to calculate the correlation coefficients between SIF and the environmental factors at both daily and half-hour scales (Figure 5). The results of a Pearson correlation analysis of the whole growing season showed that the PAR, Ta, Ws, SM and VPD had extremely significant relationships with SIF in the half-hour scale; the sequence of the correlation coefficient was $\text{PAR} > \text{VPD} > \text{Ta} > \text{Ws} > \text{SM}$. Except for the SM, all of the factors were also significantly correlated with SIF on the daily scale, and the order of the correlation coefficients was the same as on the half-hour scale. Unlike SIF, the SM had no diurnal variation. Although there was a significant correlation between SM and SIF on the half-hour scale, the correlation disappeared when the temporal aggregated to the daily scale. All the factors significantly affected the daily and half-hour scale of SIF in the spring; however, the effects of SM and Ws on SIF disappeared in the summer. SM was

correlated with the half-hour scale of SIF in the autumn, but this relationship was covered up at the daily scale.

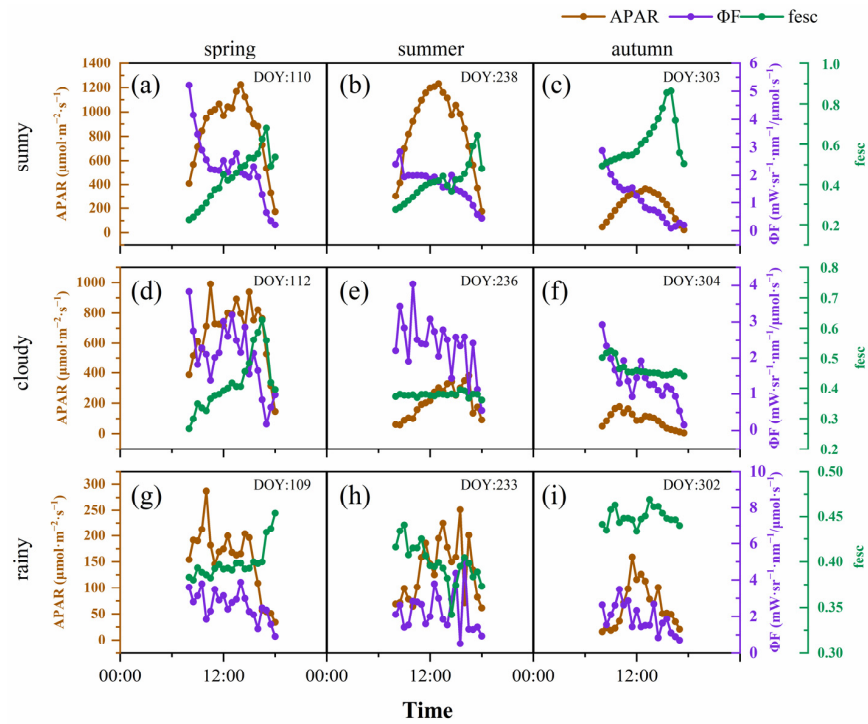


Figure 4. Diurnal dynamics of APAR (brown line); ϕF (purple line) and f_{esc} (green line) in spring (sunny (a), cloudy (d), rainy (g)); summer (sunny (b), cloudy (e), rainy (h)); and autumn (sunny (c), cloudy (f) and rainy (i)). Each subgraph was dated in the upper right corner.

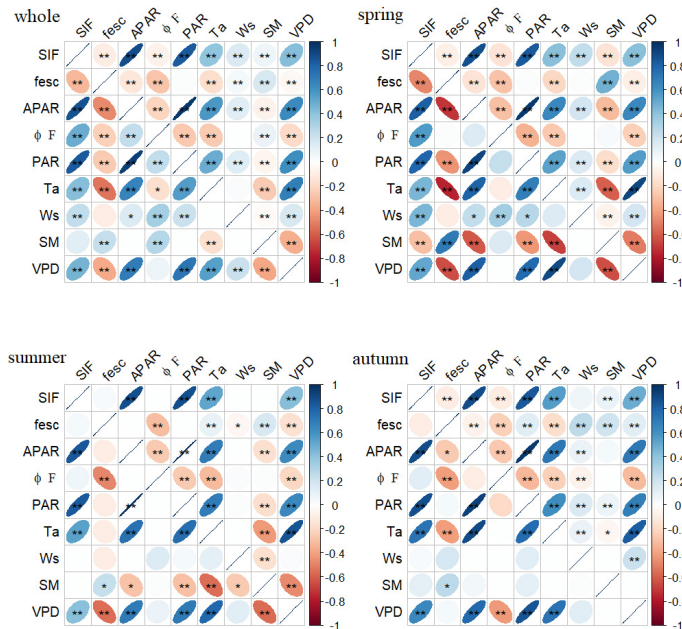


Figure 5. Pearson correlation coefficients between SIF and different environmental factors, in different seasons (whole, spring, summer and autumn). Environmental variations included PAR, Ta, wind speed (Ws), SM and VPD at daily scale (the lower part of each figure) and half-hour scale (the upper part of each figure). Blue means positive correlation; red means negative correlation; and the flatter the ellipse, the stronger the correlation. Note: *—significant correlation at $p < 0.05$ and **—significant correlation at $p < 0.01$.

PAR was a necessary condition for the emission of SIF, which was significantly correlated with SIF and APAR on both the daily and half-hour scales. It should be noted that the Ta and VPD were also significantly correlated with PAR at different temporal scales, and the correlation coefficients were larger than those between these environmental factors with SIF and APAR. In other words, the Ta, VPD, SIF and APAR had a covariant relationship with PAR, which would affect the relationship between the environmental factors and the fluorescence parameters. To eliminate this effect, we chose a partial correlation analysis to analyze the links between the fluorescence parameters with the Ta and VPD, and we took PAR as the control variable (Figure 6). After removing the effect of PAR, the VPD still significantly affected SIF, but the effect changed from positive to negative. The effect of Ta on SIF in the total growing season disappeared, indicating that the effect of Ta on SIF was derived from the effect of PAR on SIF. The influence of Ta on the half-hour scale of SIF in the spring and summer changed direction, and Ta only had a significant negative effect on SIF in the summer at the daily scale. That is to say, the effect of the VPD on SIF in the summer mainly comes from Ta, and the effect of the VPD on SIF in the spring and autumn mainly comes from RH. From the perspective of the total growing season, a partial correlation analysis showed that, after removing the influence of PAR, the significant positive effect of Ta on SIF disappeared and the positive effect of the VPD on SIF became negative.

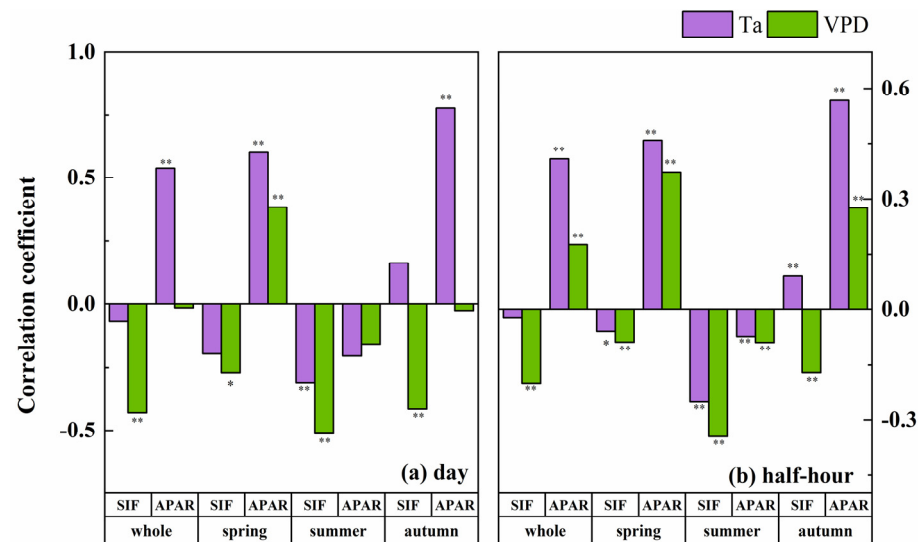


Figure 6. The partial correlation coefficient between different seasonal fluorescence parameters and environmental factors, including Ta (purple bar) and VPD (green bar) in different seasons at the daily (a) and half-hour (b) scales, with PAR as the control variable. Note: *—significant correlation at $p < 0.05$ and **—significant correlation at $p < 0.01$.

3.4. How Do Environmental Factors Affect SIF?

To clarify the influence mechanism of the environment on SIF, we established a reliable structural equation model based on the half-hour and daily scale of the growing season. The goodness-of-fit index (GFI), the comparative fit index (CFI) and the incremental fit index (IFI) of the obtained models were all closer to or above 0.9, and the root mean square error of approximation (RMSEA) was less than 0.2. This means that the models have high reliability. Figure 7 shows the influence of the environmental factors on the APAR, ϕF and f_{esc} . At the daily scale, the PAR, SM and Ws were not the main reasons for the $fPAR$ variation; the VPD had no significant effect on ϕF ; and the Ws and SM had no significant effect on the f_{esc} . At the half-hour scale, all five of the environmental factors had significant effects. In other words, the half-hour scale SIF was more susceptible to environmental factors. According to the influence coefficients in Tables 1 and 2, the direct influence of the environment on APAR mainly came from PAR, especially at the half-hour scale (0.938). At the same time, the environmental factors also affected APAR by changing $fPAR$. Ta and

the VPD drove the fPAR variation. The PAR and Ta affected ϕF . The SM affected the daily scale ϕF , while the VPD affected the half-hour scale of ϕF . It is worth noting that PAR had opposite effects on the two-time scales of ϕF . The total influence coefficients of Ta on the f_{esc} were -0.673 and -0.187 at the daily and half-hour scales, respectively, and Ta was the dominant factor of the f_{esc} . In addition, PAR and the VPD affected the f_{esc} at the daily scale, and the VPD and SM affected the f_{esc} at the half-hour scale.

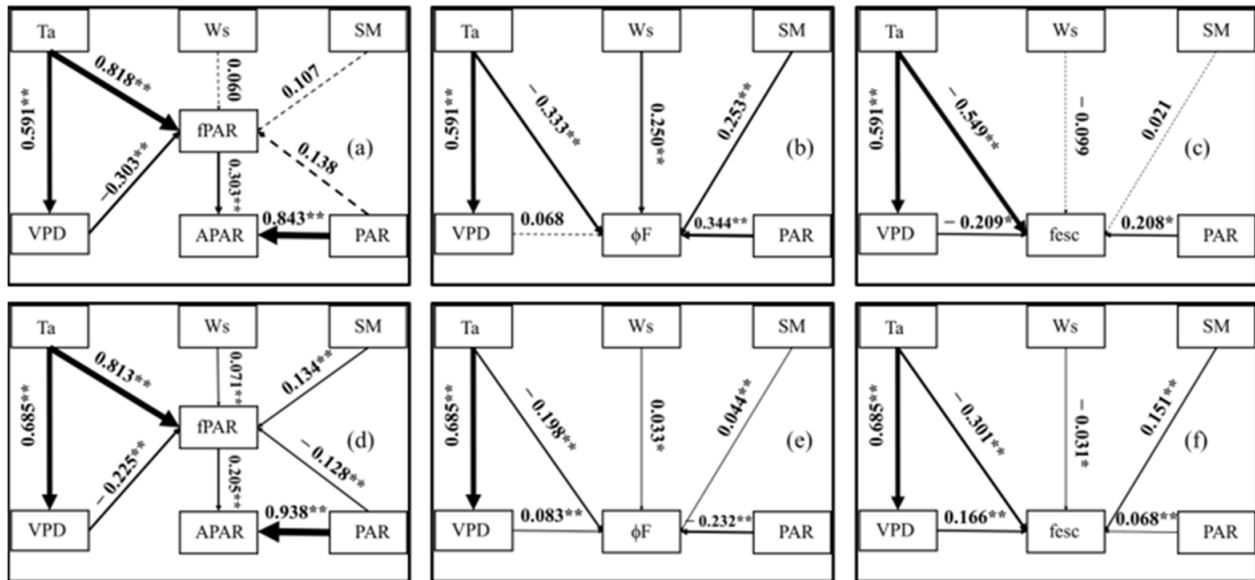


Figure 7. Structural equation model (SEM) path diagram of APAR, ϕF , f_{esc} and environmental factors in daily (a–c) and half-hour (d–f) scales. The thickness of the line represents the value of the path coefficient. All the relationships shown in the figure are significant ($p < 0.05$). The dashed line means the relationship is not significant and the solid line means the relationship is significant. Note: *—significant correlation at $p < 0.05$ and **—significant correlation at $p < 0.01$.

Table 1. The relationships between the effects of fluorescence variables and environmental variables at daily scale in the SEM.

Effect Coefficient	Variable	PAR	Ta	VPD	SM	Ws	fPAR
Standardized Direct Effects	VPD		0.591				
	fPAR	0.138	0.818	−0.303	0.107	0.06	
	APAR	0.843					0.303
	ϕF	0.344	−0.333	0.068	0.253	0.25	
	f_{esc}	0.208	−0.549	−0.209	0.021	−0.099	
Standardized Indirect Effects	VPD						
	fPAR		−0.179				
	APAR	0.042	0.194	−0.092	0.033	0.018	
	ϕF		0.04				
	f_{esc}		−0.124				
Total Effects	VPD			0.591			
	fPAR	0.138	0.639	−0.303	0.107	0.06	
	APAR	0.884	0.194	−0.092	0.033	0.018	0.303
	ϕF	0.344	−0.293	0.068	0.253	0.25	
	f_{esc}	0.208	−0.673	−0.209	0.021	−0.099	

Table 2. The relationships between the effects of fluorescence variables and environmental variables at half-hour scale in the SEM.

Effect Coefficient	Variable	PAR	Ta	VPD	SM	Ws	fPAR
Standardized Direct Effects	VPD		0.685				
	fPAR	−0.128	0.813	−0.225	0.134	0.071	
	APAR	0.938					0.205
	ϕF	−0.232	−0.198	0.083	0.044	0.033	
	f_{esc}	0.068	−0.301	0.166	0.151	0.031	
Standardized Indirect Effects	VPD						
	fPAR		−0.154				
	APAR	−0.026	0.135	−0.046	0.027	0.014	
	ϕF		0.057				
	f_{esc}		0.114				
Total Effects	VPD		0.685				
	fPAR	−0.128	0.659	−0.225	0.134	0.071	
	APAR	0.912	0.135	−0.046	0.027	0.014	0.205
	ϕF	−0.232	−0.142	0.083	0.044	0.033	
	f_{esc}	0.068	−0.187	0.166	0.151	0.031	

4. Discussion

As a reliable substitute for photosynthesis rate, SIF has been used in several research studies, with various spatio-temporal scales and ecosystems. Due to the low temporal resolution, most of the results of the current analyses of the relationships between SIF data based on satellite remote sensing and the environmental factors are not desired. Although the research that has been conducted into the leaf scale can explain some issues from a mechanistic perspective, it is doubtful whether the interpretation of individual leaves can represent the whole canopy. To clarify the influence process of the environmental factors on the canopy SIF of forest ecosystems, in this study, data on the SIF of a Chinese cork oak plantation during 2020 were continuously collected by a tower-based fluorescence automatic observation system. We analyzed these data collectively, using five environmental factors. The results showed that SIF was not only affected by PAR, but also by the VPD, SM, and other factors. This finding is crucial in properly understanding the relationship of SIF to other physiological processes, under different conditions.

4.1. The Temporal Variation Characteristic of SIF

After vegetation absorbs PAR, fluorescence is emitted from the leaves, which is finally observed at the top of the canopy through scattering and reabsorption within the canopy [68]. These processes are mainly affected by the canopy structure, the chlorophyll content and the environmental conditions [69]. The influence of the canopy structure on SIF is mainly reflected in two processes: radiation absorption (fPAR) and scattering and reabsorption (f_{esc}) [70]. In this study, the canopy SIF in a Chinese cork oak plantation showed an obvious seasonal dynamic and showed a general trend of first increasing and then decreasing in the growing season (Figure 1). Similar trends have been observed in studies on farmlands and temperate mixed forests [18,19]. As a deciduous forest, the Chinese cork oak plantation showed dramatic changes in its canopy structure, especially during the periods of leaf expansion and defoliation. The fPAR and the f_{esc} of the Chinese cork oak had obvious seasonal characteristics. The f_{esc} was mainly affected by the canopy structure and was weakly affected by the chlorophyll content. The seasonal trend and the variation amplitude of the fPAR were between the MTCI and NDVI, indicating that the fPAR was affected by a combination of the canopy structure and the chlorophyll content. The SIF in mixed forests and farmlands have been seen to decrease with the plants' senescence [12]. Vegetation usually enters the senescence stage before the deciduous stage begins. At this stage, the photosynthetic activity of the leaves decreases, accompanied by chlorophyll

decomposition to protect the photosynthetic structure from the destruction of excess light energy [71]. Chlorophyll also affects the canopy f_{esc} and the $fPAR$. Overall, the chlorophyll content affects every stage, from radiation absorption to fluorescence signal acquisition. The increase in the chlorophyll content promotes photosynthesis and fluorescence emission, leading to an increase in the SIF and maximum carboxylation rate [72]. The fluorescence yield of wheat leaves has shown a stable trend seasonally, but has also shown a decrease consistent with the chlorophyll content in the late senescence [73]. The secretion of abscisic acid, which can induce stomatal closure, is a self-protection strategy in senescence-period plants, which is often accompanied by chlorophyll decomposition. During this period, the SIF and photochemical reactions decrease and NPQ increases [74]. The influence of the canopy structure on the seasonal dynamics of SIF has been seen to be greater than that of the chlorophyll content. However, other research studies have found that there are similar trends in coniferous forests, with little seasonal variation in canopy structures. The canopy structures of coniferous forests have been seen to be basically stable throughout the year, and the chlorophyll content and temperature were seen to be the main causes of seasonal changes [75]. The decrease in SIF in the winter has been observed as due to the seasonal physiological changes mediated by photochemical quenching and non-photochemical quenching [3].

Under sunny conditions, the diurnal variation of the SIF has shown a “unimodal” pattern, which was similar to the diurnal dynamics of PAR [76,77]. As we know, plant photosynthesis is prone to midday inhibition during sunny days. In fact, due to the pressure of high T_a or high VPD, chlorophyll fluorescence at the leaf-scale has occurred as a phenomenon similar to photosynthetic midday depression. In their research on temperate forests, Lu et al. found that there was midday inhibition of fluorescence after they ignored the canopy scattering and reabsorption processes [19]. In this study, top-canopy leaves may have occurred midday inhibition under direct sunlight and high VPD conditions, while inner-canopy leaves were not stressed due to the canopy shading or microclimate. The tower-based system collected fluorescence throughout the canopy, so the leaves inside the canopy were full of this inhibition, which may have been one reason for the absence of midday inhibition. Another possibility is that Chinese cork oak is a drought-resistant species and, thus, the environmental conditions did not reach the threshold for inhibition during the observation period. By observing the diurnal variation trend, we found that the SIF changed asymmetrically in the morning and afternoon, even under the condition of symmetrical PAR. Other research studies on crops have concluded that the asymmetry was caused by the obvious row structure of farmland, and further research has found that the diurnal variation of maize-canopy SIF was caused by the variation of incident solar radiation and solar observation geometry [78]. The zenith angle can change the ratio of sun and shade leaves, thus changing the observed canopy structure [79]. The f_{esc} is affected by the LAI and the leaf inclination angle distribution, and the growth differences, water stress and wind direction lead to uneven distribution and variation in the canopy geometry [19]. Therefore, in this study, the f_{esc} in the afternoon was higher than that in the morning (Figure 4), which may have been caused by changes in the canopy structure, zenith angle and leaf movement, and the asymmetry of APAR also confirmed this possibility. The diurnal inflection points of SIF on the sunny days gradually advanced with the advance in growth; however, this was not found on cloudy and rainy days. Clouds will reduce the total solar radiation and increase the diffuse reflection, possibly greatly reducing the effect of the zenith angle on the f_{esc} . The f_{esc} changed slightly on cloudy and rainy days, which may be the reason why the relationship between SIF and GPP on cloudy days was closer than it was on sunny days.

4.2. Regulation of SIF by Environmental Factors

In the daily scale, SIF was not only affected by the canopy structure and pigment content, but also fluctuated according to the environmental factors. This was especially true when the canopy structure was stable, as environmental factors dominated the dynamics of

SIF. SIF contains information about APAR and the environmental stresses (e.g., temperature and water stress) related to photosynthetic light energy utilization [14,80]. Compared with the vegetation index, SIF had more obvious daily dynamics and was more sensitive to the variations in PAR, Ta, VPD and SM [69,81]. To clarify the influence path of the environmental factors on SIF, we analyzed the responses of the APAR, ϕF and the f_{esc} to the PAR, Ta, VPD, SM and Ws. The results showed that PAR was the most closely related factor to the SIF in the Chinese cork oak canopy, which significantly affected the three components in most cases, indicating that the SIF was driven by incident solar radiation. The ability of PAR to drive SIF has been recognized in many studies [82–85]. However, there is another explanation for what drives the diurnal dynamic of SIF: the genes that encode the chlorophyll binding proteins may be up-regulated at dawn and down-regulated before sunset [86]. This suggests that the circadian rhythm may be another factor in determining the dynamics and in changing the relationship between fluorescence and photosynthesis. The opposite effect of PAR on ϕF at two time-scales may be related to the diurnal dynamics of PAR. When PAR exceeds the electron transport chain capacity, plants will protect their leaf structure through NPQ [87], which will reduce their fluorescence yield [88,89]. The analysis of the relationship between the environmental factors (e.g., PAR, Ta and precipitation) and the forest SIF, which was based on remote sensing data, found that the 16-day and day-scale SIF in the Greater Khingan Mountains were only related to the Ta [30]. The satellite data were instantaneous, taken from one moment in time, and thus, they did not include the diurnal dynamics of PAR. In this condition, there was no significant relationship between SIF and PAR, suggesting that the circadian rhythm could affect this relationship. On a regional scale, the Ta regulated SIF by influencing photosynthesis.

We found that the Ta had a consistent and significant effect on SIF. It had a positive effect on APAR and a negative effect on the ϕF and f_{esc} , yet the contribution of APAR to SIF was higher than that of ϕF and the f_{esc} ; therefore, the Ta had a positive effect on SIF. After eliminating the covariant of Ta and PAR, the effect of the Ta on the daily SIF was weakened or had disappeared. In the spring and summer, the Ta was higher than the optimum photosynthetic temperature, and it had a negative effect on SIF. High temperatures reduce the photosynthetic rate, and radiation promotes the temperature; therefore, the compensation of PAR to SIF covered the inhibition effect of the high temperatures on SIF. While the temperature in autumn was low, Ta became a photosynthetic limiting factor and influenced the rhythm of the vegetation [75]. The soil moisture of this study site was insufficient and the change of intra-day Ta impacted on leaf morphology (high temperature will make the leaf curl), which may be the reason why Ta significantly affected f_{esc} at the half-hour scale [90]. The reasons for the significant influence of Ta on f_{esc} at a daily scale can be explained from two aspects. On the one hand, Ta was related to the canopy structure through synergistic changes with the phenological pattern in deciduous broadleaf forest. On the other hand, continuous high Ta along with less precipitation in May–June (late spring and early summer) regulated canopy structure. In addition, the decline rate of MTCI in September–October was higher than that in NDVI (Figure 1), indicating that the decrease of Ta in autumn led to the decomposition of leaf chlorophyll [91], which could be another reason why Ta affected f_{esc} . The environment not only affected SIF directly by changing the allocation of the light energy, but also indirectly by regulating stomatal behavior. Plant stomata are accesses that regulate and control photosynthesis and transpiration. Some physiological processes also require stomata for gas exchange. Stomata are closed at night, even when the temperature and water are optimal for plants; light is the necessary condition for the stomata to open. Circadian rhythm can affect the relationship between photosynthesis and fluorescence efficiency by controlling stomatal conductance [92]. The VPD is an indicator of meteorological drought, and leaf curl/stretch can change canopy structures (f_{esc}) to affect SIF. Moreover, the VPD can affect stomatal opening and closing; however, this effect was mainly reflected in the half-hour scale. Previous research has shown that the influence of the VPD on SIF had a critical value; thus, a high VPD will have a negative effect on SIF [93]. Our results showed that the VPD had a positive effect on SIF

(Figure 5). However, after removing the covariant effect of the VPD and PAR, VPD had a negative effect on SIF (Figure 6). PAR mutated the effect of the VPD on SIF, and the asynchronous response of SIF and the GPP to the VPD may be one of the reasons for decoupling in drought events. W_s affected SIF in physical and physiological directions. First, wind affected the canopy structure by moving or rolling the blades, causing changes in APAR (half-hour). Second, the wind affected stomatal conductance by changing transpiration pull, causing changes in light utilization.

5. Conclusions

In this study, continuous and synchronous observations of canopy SIF and environmental factors were made in Chinese cork oak, in 2020. We found that canopy SIF had distinct seasonal and diurnal dynamics, which were mainly driven by PAR. The obvious variation in the f_{esc} in the intra-day may be the main reason for the asymmetry of the diurnal variation of SIF on sunny days. PAR, T_a , VPD and W_s significantly affected the daily and half-hour scale SIF during the growing season. The correlation between SM and SIF was robust during the spring and autumn, when the precipitation was low, but not significant in the summer. After eliminating the covariant effect of PAR with T_a and the VPD, the relationship between T_a and SIF in the total growing season disappeared due to the different effects of T_a on SIF in the different seasons. The effect of the VPD on SIF was negative. This study showed that the influence of environmental factors related to water and heat on SIF varied with the seasons. In relatively dry seasons, the SM and VPD have more significant effects on SIF through the canopy structure and fluorescence yield. In the autumn, when the leaves were aging and the temperature was low, T_a became a photosynthetic-limiting factor and promoted SIF by affecting the fluorescence yield. This study further clarified the response mechanism of SIF to environmental factors, providing a basis for analyzing the differences between SIF and photosynthesis in the coping strategies necessary for climate change. It would be helpful for subsequent research to investigate or predict the relationship between SIF and the GPP under different conditions and to understand the possible causes of this.

Author Contributions: Conceptualization, J.Z. and H.H.; methodology, M.H. and X.C.; software, M.H. and Y.Z.; validation, X.W. and Q.P.; writing—original draft preparation, M.H.; writing—review and editing, J.Z. and C.G.; visualization, M.H.; supervision, J.Z. and H.H.; funding acquisition, J.Z. All authors have read and agreed to the published version of the manuscript.

Funding: This study was funded by grant number CAFYBB2020QD002–2.

Data Availability Statement: The datasets generated during and/or analyzed during the current study are available from the corresponding author on reasonable request.

Acknowledgments: The authors thank the staff of the Henan Xiaolangdi Earth Critical Zone National Research Station on the Middle Yellow River for their support and help in the field experiment.

Conflicts of Interest: The authors declare no conflict of interest.

References

1. Xu, G.; Liu, X.; Trouet, V.; Treydte, K.; Wu, G.; Chen, T.; Sun, W.; An, W.; Wang, W.; Zeng, X. Regional drought shifts (1710–2010) in East Central Asia and linkages with atmospheric circulation recorded in tree-ring $\delta^{18}O$. *Clim. Dyn.* **2019**, *52*, 713–727. [[CrossRef](#)]
2. Jiao, L.; Jiang, Y.; Zhang, W.; Wang, M.; Wang, S.; Liu, X. Assessing the stability of radial growth responses to climate change by two dominant conifer trees species in the Tianshan Mountains, northwest China. *For. Ecol. Manag.* **2019**, *433*, 667–677. [[CrossRef](#)]
3. Magney, T.; Bowling, D.; Logan, B.; Grossmann, K.; Stutz, J.; Blanken, P.; Burns, S.; Cheng, R.; Garcia, M.; Köhler, P. Mechanistic evidence for tracking the seasonality of photosynthesis with solar-induced fluorescence. *Proc. Natl. Acad. Sci. USA* **2019**, *116*, 11640–11645. [[CrossRef](#)] [[PubMed](#)]
4. Shen, M.; Piao, S.; Jeong, S.-J.; Zhou, L.; Zeng, Z.; Ciais, P.; Chen, D.; Huang, M.; Jin, C.; Li, L.Z. Evaporative cooling over the Tibetan Plateau induced by vegetation growth. *Proc. Natl. Acad. Sci. USA* **2015**, *112*, 9299–9304. [[CrossRef](#)] [[PubMed](#)]
5. Lian, X.; Jeong, S.; Park, C.; Xu, H.; Li, L.; Wang, T.; Gentine, P.; Peñuelas, J.; Piao, S. Biophysical impacts of northern vegetation changes on seasonal warming patterns. *Nat. Commun.* **2022**, *13*, 3925. [[CrossRef](#)]

6. Zhang, Y.; Xiao, X.; Wu, X.; Zhou, S.; Zhang, G.; Qin, Y.; Dong, J. A global moderate resolution dataset of gross primary production of vegetation for 2000–2016. *Sci. Data* **2017**, *4*, 170165. [[CrossRef](#)] [[PubMed](#)]
7. Ryu, Y.; Baldocchi, D.; Black, T.; Detto, M.; Law, B.; Leuning, R.; Miyata, A.; Reichstein, M.; Vargas, R.; Ammann, C. On the temporal upscaling of evapotranspiration from instantaneous remote sensing measurements to 8-day mean daily-sums. *Agric. For. Meteorol.* **2012**, *152*, 212–222. [[CrossRef](#)]
8. Wu, C.; Han, X.; Ni, J.; Niu, Z.; Huang, W. Estimation of gross primary production in wheat from in situ measurements. *Int. J. Appl. Earth Obs. Geoinf.* **2010**, *12*, 183–189. [[CrossRef](#)]
9. Wu, G.; Guan, K.; Jiang, C.; Peng, B.; Kimm, H.; Chen, M.; Yang, X.; Wang, S.; Suyker, A.E.; Bernacchi, C.J. Radiance-based NIRv as a proxy for GPP of corn and soybean. *Environ. Res. Lett.* **2020**, *15*, 034009. [[CrossRef](#)]
10. Porcar-Castell, A.; Tyystjärvi, E.; Atherton, J.; Van der Tol, C.; Flexas, J.; Pfündel, E.E.; Moreno, J.; Frankenberg, C.; Berry, J.A. Linking chlorophyll a fluorescence to photosynthesis for remote sensing applications: Mechanisms and challenges. *J. Exp. Bot.* **2014**, *65*, 4065–4095. [[CrossRef](#)]
11. Mohammed, G.H.; Colombo, R.; Middleton, E.M.; Rascher, U.; van der Tol, C.; Nedbal, L.; Goulas, Y.; Pérez-Priego, O.; Damm, A.; Meroni, M. Remote sensing of solar-induced chlorophyll fluorescence (SIF) in vegetation: 50 years of progress. *Remote Sens. Environ.* **2019**, *231*, 111177. [[CrossRef](#)] [[PubMed](#)]
12. Wang, F.; Chen, B.; Lin, X.; Zhang, H. Solar-induced chlorophyll fluorescence as an indicator for determining the end date of the vegetation growing season. *Ecol. Indic.* **2020**, *109*, 105755. [[CrossRef](#)]
13. Magney, T.S.; Frankenberg, C.; Fisher, J.B.; Sun, Y.; North, G.B.; Davis, T.S.; Kornfeld, A.; Siebke, K. Connecting active to passive fluorescence with photosynthesis: A method for evaluating remote sensing measurements of Chl fluorescence. *New Phytol.* **2017**, *215*, 1594–1608. [[CrossRef](#)]
14. Li, X.; Xiao, J.; He, B.; Altaf Arain, M.; Beringer, J.; Desai, A.R.; Emmel, C.; Hollinger, D.Y.; Krasnova, A.; Mammarella, I. Solar-induced chlorophyll fluorescence is strongly correlated with terrestrial photosynthesis for a wide variety of biomes: First global analysis based on OCO-2 and flux tower observations. *Glob. Change Biol.* **2018**, *24*, 3990–4008. [[CrossRef](#)] [[PubMed](#)]
15. Zhang, L.; Shen, M.; Jiang, N.; Lv, J.; Liu, L.; Zhang, L. Spatial variations in the response of spring onset of photosynthesis of evergreen vegetation to climate factors across the Tibetan Plateau: The roles of interactions between temperature, precipitation, and solar radiation. *Agric. For. Meteorol.* **2023**, *335*, 109440. [[CrossRef](#)]
16. Wood, J.D.; Griffis, T.J.; Baker, J.M.; Frankenberg, C.; Verma, M.; Yuen, K. Multiscale analyses of solar-induced fluorescence and gross primary production. *Geophys. Res. Lett.* **2017**, *44*, 533–541. [[CrossRef](#)]
17. Jeong, S.; Schimel, D.; Frankenberg, C.; Drewry, D.; Fisher, J.; Verma, M.; Berry, J.; Lee, J.; Joiner, J. Application of satellite solar-induced chlorophyll fluorescence to understanding large-scale variations in vegetation phenology and function over northern high latitude forests. *Remote Sens. Environ.* **2017**, *190*, 178–187. [[CrossRef](#)]
18. Dechant, B.; Ryu, Y.; Badgley, G.; Zeng, Y.; Berry, J.A.; Zhang, Y.; Goulas, Y.; Li, Z.; Zhang, Q.; Kang, M. Canopy structure explains the relationship between photosynthesis and sun-induced chlorophyll fluorescence in crops. *Remote Sens. Environ.* **2020**, *241*, 111733. [[CrossRef](#)]
19. Lu, X.; Liu, Z.; Zhao, F.; Tang, J. Comparison of total emitted solar-induced chlorophyll fluorescence (SIF) and top-of-canopy (TOC) SIF in estimating photosynthesis. *Remote Sens. Environ.* **2020**, *251*, 112083. [[CrossRef](#)]
20. Bendig, J.; Malenovsky, Z.; Gautam, D.; Lucieer, A. Solar-induced chlorophyll fluorescence measured from an unmanned aircraft system: Sensor etaloning and platform motion correction. *IEEE Trans. Geosci. Remote Sens.* **2019**, *58*, 3437–3444. [[CrossRef](#)]
21. Chang, C.; Zhou, R.; Kira, O.; Marri, S.; Skovira, J.; Gu, L.; Sun, Y. An Unmanned Aerial System (UAS) for concurrent measurements of solar-induced chlorophyll fluorescence and hyperspectral reflectance toward improving crop monitoring. *Agric. For. Meteorol.* **2020**, *294*, 108145. [[CrossRef](#)]
22. Kira, O.; Sun, Y. Extraction of sub-pixel C3/C4 emissions of solar-induced chlorophyll fluorescence (SIF) using artificial neural network. *ISPRS J. Photogramm. Remote Sens.* **2020**, *161*, 135–146. [[CrossRef](#)]
23. Grossmann, K.; Frankenberg, C.; Magney, T.S.; Hurlock, S.C.; Seibt, U.; Stutz, J. PhotoSpec: A new instrument to measure spatially distributed red and far-red Solar-Induced Chlorophyll Fluorescence. *Remote Sens. Environ.* **2018**, *216*, 311–327. [[CrossRef](#)]
24. Zhang, Q.; Zhang, X.; Li, Z.; Wu, Y.; Zhang, Y. Comparison of Bi-hemispherical and hemispherical-conical configurations for in situ measurements of solar-induced chlorophyll fluorescence. *Remote Sens.* **2019**, *11*, 2642. [[CrossRef](#)]
25. Gu, L.; Wood, J.; Chang, C.; Sun, Y.; Riggs, J. Advancing terrestrial ecosystem science with a novel automated measurement system for sun-induced chlorophyll fluorescence for integration with eddy covariance flux networks. *J. Geophys. Res. Biogeosci.* **2019**, *124*, 127–146. [[CrossRef](#)]
26. Liu, Z.; Zhao, F.; Liu, X.; Yu, Q.; Wang, Y.; Peng, X.; Cai, H.; Lu, X. Direct estimation of photosynthetic CO₂ assimilation from solar-induced chlorophyll fluorescence (SIF). *Remote Sens. Environ.* **2022**, *271*, 112893. [[CrossRef](#)]
27. Qiu, B.; Chen, J.M.; Ju, W.; Zhang, Q.; Zhang, Y. Simulating emission and scattering of solar-induced chlorophyll fluorescence at far-red band in global vegetation with different canopy structures. *Remote Sens. Environ.* **2019**, *233*, 111373. [[CrossRef](#)]
28. Zhang, Y.; Zhang, Q.; Liu, L.; Zhang, Y.; Wang, S.; Ju, W.; Zhou, G.; Zhou, L.; Tang, J.; Zhu, X. ChinaSpec: A Network for Long-Term Ground-Based Measurements of Solar-Induced Fluorescence in China. *J. Geophys. Res. Biogeosci.* **2021**, *126*, e2020JG006042. [[CrossRef](#)]
29. Baker, N.R. Chlorophyll fluorescence: A probe of photosynthesis in vivo. *Annu. Rev. Plant Biol.* **2008**, *59*, 89–113. [[CrossRef](#)]

30. Guo, M.; Li, J.; Huang, S.; Wen, L. Feasibility of using MODIS products to simulate sun-induced chlorophyll fluorescence (SIF) in boreal forests. *Remote Sens.* **2020**, *12*, 680. [[CrossRef](#)]
31. Pierrat, Z.; Magney, T.; Parazoo, N.; Grossmann, K.; Bowling, D.; Seibt, U.; Johnson, B.; Helgason, W.; Barr, A.; Bortnik, J. Diurnal and seasonal dynamics of solar-induced chlorophyll fluorescence, vegetation indices, and gross primary productivity in the boreal forest. *J. Geophys. Res. Biogeosci.* **2022**, *127*, e2021JG006588. [[CrossRef](#)]
32. Wu, G.; Guan, K.; Jiang, C.; Kimm, H.; Miao, G.; Bernacchi, C.J.; Moore, C.E.; Ainsworth, E.A.; Yang, X.; Berry, J.A. Attributing differences of solar-induced chlorophyll fluorescence (SIF)-gross primary production (GPP) relationships between two C4 crops: Corn and miscanthus. *Agric. For. Meteorol.* **2022**, *323*, 109046. [[CrossRef](#)]
33. Grieu, P.; Guehl, J.; Aussenac, G. The effects of soil and atmospheric drought on photosynthesis and stomatal control of gas exchange in three coniferous species. *Physiol. Plant.* **1988**, *73*, 97–104. [[CrossRef](#)]
34. Fletcher, A.L.; Sinclair, T.R.; Allen Jr, L.H. Transpiration responses to vapor pressure deficit in well watered 'slow-wilting' and commercial soybean. *Environ. Exp. Bot.* **2007**, *61*, 145–151. [[CrossRef](#)]
35. Liu, L.; Teng, Y.; Wu, J.; Zhao, W.; Liu, S.; Shen, Q. Soil water deficit promotes the effect of atmospheric water deficit on solar-induced chlorophyll fluorescence. *Sci. Total Environ.* **2020**, *720*, 137408. [[CrossRef](#)]
36. Porcar-Castell, A.; Malenovsky, Z.; Magney, T.; Van Wittenberghe, S.; Fernández-Marín, B.; Maignan, F.; Zhang, Y.; Maseyk, K.; Atherton, J.; Albert, L.P. Chlorophyll a fluorescence illuminates a path connecting plant molecular biology to Earth-system science. *Nat. Plants* **2021**, *7*, 998–1009. [[CrossRef](#)]
37. Zhang, Z.; Zhang, Y.; Porcar-Castell, A.; Joiner, J.; Guanter, L.; Yang, X.; Migliavacca, M.; Ju, W.; Sun, Z.; Chen, S. Reduction of structural impacts and distinction of photosynthetic pathways in a global estimation of GPP from space-borne solar-induced chlorophyll fluorescence. *Remote Sens. Environ.* **2020**, *240*, 111722. [[CrossRef](#)]
38. Rossini, M.; Meroni, M.; Celesti, M.; Cogliati, S.; Julitta, T.; Panigada, C.; Rascher, U.; Van der Tol, C.; Colombo, R. Analysis of red and far-red sun-induced chlorophyll fluorescence and their ratio in different canopies based on observed and modeled data. *Remote Sens.* **2016**, *8*, 412. [[CrossRef](#)]
39. Björkman, O.; Demmig, B. Photon yield of O₂ evolution and chlorophyll fluorescence characteristics at 77 K among vascular plants of diverse origins. *Planta* **1987**, *170*, 489–504. [[CrossRef](#)]
40. Lin, Y.; Hu, Y.; Ren, C.; Guo, L.; Wang, C.; Jiang, Y.; Wang, X.; Phendukani, H.; Zeng, Z. Effects of nitrogen application on chlorophyll fluorescence parameters and leaf gas exchange in naked oat. *J. Integr. Agric.* **2013**, *12*, 2164–2171. [[CrossRef](#)]
41. Badgley, G.; Field, C.B.; Berry, J.A. Canopy near-infrared reflectance and terrestrial photosynthesis. *Sci. Adv.* **2017**, *3*, e1602244. [[CrossRef](#)] [[PubMed](#)]
42. Rogers, C.A.; Chen, J.M. Land cover and latitude affect vegetation phenology determined from solar induced fluorescence across Ontario, Canada. *Int. J. Appl. Earth Obs. Geoinf.* **2022**, *114*, 103036. [[CrossRef](#)]
43. Zhang, J.; Xiao, J.; Tong, X.; Zhang, J.; Meng, P.; Li, J.; Liu, P.; Yu, P. NIRv and SIF better estimate phenology than NDVI and EVI: Effects of spring and autumn phenology on ecosystem production of planted forests. *Agric. For. Meteorol.* **2022**, *315*, 108819. [[CrossRef](#)]
44. Paul-Limoges, E.; Damm, A.; Hueni, A.; Liebisch, F.; Eugster, W.; Schaepman, M.E.; Buchmann, N. Effect of environmental conditions on sun-induced fluorescence in a mixed forest and a cropland. *Remote Sens. Environ.* **2018**, *219*, 310–323. [[CrossRef](#)]
45. Migliavacca, M.; Perez-Priego, O.; Rossini, M.; El-Madany, T.S.; Moreno, G.; Van der Tol, C.; Rascher, U.; Berninger, A.; Bessenbacher, V.; Burkart, A. Plant functional traits and canopy structure control the relationship between photosynthetic CO₂ uptake and far-red sun-induced fluorescence in a Mediterranean grassland under different nutrient availability. *New Phytol.* **2017**, *214*, 1078–1091. [[CrossRef](#)]
46. Yang, P.; van der Tol, C.; Verhoef, W.; Damm, A.; Schickling, A.; Kraska, T.; Muller, O.; Rascher, U. Using reflectance to explain vegetation biochemical and structural effects on sun-induced chlorophyll fluorescence. *Remote Sens. Environ.* **2019**, *231*, 110996. [[CrossRef](#)]
47. Chang, C.Y.; Wen, J.; Han, J.; Kira, O.; LeVonne, J.; Melkonian, J.; Riha, S.J.; Skovira, J.; Ng, S.; Gu, L. Unpacking the drivers of diurnal dynamics of sun-induced chlorophyll fluorescence (SIF): Canopy structure, plant physiology, instrument configuration and retrieval methods. *Remote Sens. Environ.* **2021**, *265*, 112672. [[CrossRef](#)]
48. Yáñez-Rausell, L.; Schaepman, M.E.; Clevers, J.G.; Malenovsky, Z. Minimizing measurement uncertainties of coniferous needle-leaf optical properties, Part I: Methodological review. *IEEE J. Sel. Top. Appl. Earth Obs. Remote Sens.* **2013**, *7*, 399–405. [[CrossRef](#)]
49. Middleton, E.M.; Cheng, Y.-B.; Corp, L.A.; Campbell, P.K.; Huemmrich, K.F.; Zhang, Q.; Kustas, W.P. Canopy Level Chlorophyll Fluorescence and the PRI in a Cornfield. In Proceedings of the 2012 IEEE International Geoscience and Remote Sensing Symposium, Munich, Germany, 22–27 July 2012; pp. 7117–7120.
50. Guo, M.; Li, J.; Li, J.; Zhong, C.; Zhou, F. Solar-Induced Chlorophyll Fluorescence Trends and Mechanisms in Different Ecosystems in Northeastern China. *Remote Sens.* **2022**, *14*, 1329. [[CrossRef](#)]
51. Zhou, K.; Zhang, Q.; Xiong, L.; Gentine, P. Estimating evapotranspiration using remotely sensed solar-induced fluorescence measurements. *Agric. For. Meteorol.* **2022**, *314*, 108800. [[CrossRef](#)]
52. Wang, Y.; Frankenberg, C. On the impact of canopy model complexity on simulated carbon, water, and solar-induced chlorophyll fluorescence fluxes. *Biogeosciences* **2022**, *19*, 29–45. [[CrossRef](#)]

53. Tagliabue, G.; Panigada, C.; Celesti, M.; Cogliati, S.; Colombo, R.; Migliavacca, M.; Rascher, U.; Rocchini, D.; Schüttemeyer, D.; Rossini, M. Sun-induced fluorescence heterogeneity as a measure of functional diversity. *Remote Sens. Environ.* **2020**, *247*, 111934. [[CrossRef](#)]
54. Allen, R.G.; Pereira, L.S.; Raes, D.; Smith, M. *Crop Evapotranspiration-Guidelines for Computing Crop Water Requirements-FAO Irrigation and Drainage Paper 56*; FAO: Rome, Italy, 1998; Volume 300, p. D05109.
55. Mazzoni, M.; Falorni, P.; Del Bianco, S. Sun-induced leaf fluorescence retrieval in the O₂-B atmospheric absorption band. *Opt. Express* **2008**, *16*, 7014–7022. [[CrossRef](#)] [[PubMed](#)]
56. Cui, Z.; Kerekes, J.P. Impact of wavelength shift in relative spectral response at high angles of incidence in landsat-8 operational land imager and future landsat design concepts. *IEEE Trans. Geosci. Remote Sens.* **2018**, *56*, 5873–5883. [[CrossRef](#)]
57. Cui, Z.; Kerekes, J.P. Potential of red edge spectral bands in future landsat satellites on agroecosystem canopy green leaf area index retrieval. *Remote Sens.* **2018**, *10*, 1458. [[CrossRef](#)]
58. Rouse, J.W.; Haas, R.H.; Schell, J.A.; Deering, D.W. Monitoring vegetation systems in the Great Plains with ERTS. *NASA Spec. Publ.* **1974**, *351*, 309.
59. Viña, A.; Gitelson, A.A.; Nguy-Robertson, A.L.; Peng, Y. Comparison of different vegetation indices for the remote assessment of green leaf area index of crops. *Remote Sens. Environ.* **2011**, *115*, 3468–3478. [[CrossRef](#)]
60. Dash, J.; Curran, P. The MERIS terrestrial chlorophyll index. *Int. J. Remote Sens.* **2004**, *25*, 5403–5413. [[CrossRef](#)]
61. Viña, A.; Gitelson, A.A. New developments in the remote estimation of the fraction of absorbed photosynthetically active radiation in crops. *Geophys. Res. Lett.* **2005**, *32*, L17403. [[CrossRef](#)]
62. Miao, G.; Guan, K.; Yang, X.; Bernacchi, C.J.; Berry, J.A.; DeLucia, E.H.; Wu, J.; Moore, C.E.; Meacham, K.; Cai, Y. Sun-induced chlorophyll fluorescence, photosynthesis, and light use efficiency of a soybean field from seasonally continuous measurements. *J. Geophys. Res. Biogeosci.* **2018**, *123*, 610–623. [[CrossRef](#)]
63. Zhang, Y.; Xiao, X.; Wolf, S.; Wu, J.; Wu, X.; Gioli, B.; Wohlfahrt, G.; Cescatti, A.; Van der Tol, C.; Zhou, S. Spatio-temporal convergence of maximum daily light-use efficiency based on radiation absorption by canopy chlorophyll. *Geophys. Res. Lett.* **2018**, *45*, 3508–3519. [[CrossRef](#)]
64. Zeng, Y.; Badgley, G.; Dechant, B.; Ryu, Y.; Chen, M.; Berry, J.A. A practical approach for estimating the escape ratio of near-infrared solar-induced chlorophyll fluorescence. *Remote Sens. Environ.* **2019**, *232*, 111209. [[CrossRef](#)]
65. Kumar, R.; Umanand, L. Estimation of global radiation using clearness index model for sizing photovoltaic system. *Renew. Energy* **2005**, *30*, 2221–2233. [[CrossRef](#)]
66. Gu, L.; Fuentes, J.D.; Shugart, H.H.; Staebler, R.M.; Black, T.A. Responses of net ecosystem exchanges of carbon dioxide to changes in cloudiness: Results from two North American deciduous forests. *J. Geophys. Res. Atmos.* **1999**, *104*, 31421–31434. [[CrossRef](#)]
67. Li, Z.; Zhang, Q.; Li, J.; Yang, X.; Wu, Y.; Zhang, Z.; Wang, S.; Wang, H.; Zhang, Y. Solar-induced chlorophyll fluorescence and its link to canopy photosynthesis in maize from continuous ground measurements. *Remote Sens. Environ.* **2020**, *236*, 111420. [[CrossRef](#)]
68. Yang, K.; Ryu, Y.; Dechant, B.; Berry, J.A.; Hwang, Y.; Jiang, C.; Kang, M.; Kim, J.; Kimm, H.; Kornfeld, A. Sun-induced chlorophyll fluorescence is more strongly related to absorbed light than to photosynthesis at half-hourly resolution in a rice paddy. *Remote Sens. Environ.* **2018**, *216*, 658–673. [[CrossRef](#)]
69. Li, X.; Xiao, J. Global climatic controls on interannual variability of ecosystem productivity: Similarities and differences inferred from solar-induced chlorophyll fluorescence and enhanced vegetation index. *Agric. For. Meteorol.* **2020**, *288*, 108018. [[CrossRef](#)]
70. Wu, J.; Albert, L.P.; Lopes, A.P.; Restrepo-Coupe, N.; Hayek, M.; Wiedemann, K.T.; Guan, K.; Stark, S.C.; Christoffersen, B.; Prohaska, N. Leaf development and demography explain photosynthetic seasonality in Amazon evergreen forests. *Science* **2016**, *351*, 972–976. [[CrossRef](#)]
71. Biswal, B.; Krupinska, K.; Biswal, U.C. *Plastid Development in Leaves during Growth and Senescence*; Springer: Dordrecht, The Netherlands, 2013.
72. Berry, J. 3.10 solar induced chlorophyll fluorescence: Origins, relation to photosynthesis and retrieval. *Compr. Remote Sens.* **2018**, *3*, 143–162.
73. Goulas, Y.; Fournier, A.; Daumard, F.; Champagne, S.; Ounis, A.; Marloie, O.; Moya, I. Gross primary production of a wheat canopy relates stronger to far red than to red solar-induced chlorophyll fluorescence. *Remote Sens.* **2017**, *9*, 97. [[CrossRef](#)]
74. Chaves, M.; Flexas, J.; Pinheiro, C. Photosynthesis under drought and salt stress: Regulation mechanisms from whole plant to cell. *Ann. Bot.* **2009**, *103*, 551–560. [[CrossRef](#)] [[PubMed](#)]
75. Raczka, B.; Porcar-Castell, A.; Magney, T.; Lee, J.; Köhler, P.; Frankenberg, C.; Grossmann, K.; Logan, B.; Stutz, J.; Blanken, P. Sustained nonphotochemical quenching shapes the seasonal pattern of solar-induced fluorescence at a high-elevation evergreen forest. *J. Geophys. Res. Biogeosci.* **2019**, *124*, 2005–2020. [[CrossRef](#)]
76. Yang, X.; Tang, J.; Mustard, J.F.; Lee, J.E.; Rossini, M.; Joiner, J.; Munger, J.W.; Kornfeld, A.; Richardson, A.D. Solar-induced chlorophyll fluorescence that correlates with canopy photosynthesis on diurnal and seasonal scales in a temperate deciduous forest. *Geophys. Res. Lett.* **2015**, *42*, 2977–2987. [[CrossRef](#)]
77. Liu, L.; Yang, X.; Zhou, H.; Liu, S.; Zhou, L.; Li, X.; Yang, J.; Han, X.; Wu, J. Evaluating the utility of solar-induced chlorophyll fluorescence for drought monitoring by comparison with NDVI derived from wheat canopy. *Sci. Total Environ.* **2018**, *625*, 1208–1217. [[CrossRef](#)]

78. Yang, P.; van der Tol, C.; Campbell, P.K.; Middleton, E.M. Fluorescence Correction Vegetation Index (FCVI): A physically based reflectance index to separate physiological and non-physiological information in far-red sun-induced chlorophyll fluorescence. *Remote Sens. Environ.* **2020**, *240*, 111676. [[CrossRef](#)]
79. He, L.; Chen, J.M.; Liu, J.; Mo, G.; Joiner, J. Angular normalization of GOME-2 Sun-induced chlorophyll fluorescence observation as a better proxy of vegetation productivity. *Geophys. Res. Lett.* **2017**, *44*, 5691–5699. [[CrossRef](#)]
80. Walther, S.; Voigt, M.; Thum, T.; Gonsamo, A.; Zhang, Y.; Köhler, P.; Jung, M.; Varlagin, A.; Guanter, L. Satellite chlorophyll fluorescence measurements reveal large-scale decoupling of photosynthesis and greenness dynamics in boreal evergreen forests. *Glob. Change Biol.* **2016**, *22*, 2979–2996. [[CrossRef](#)]
81. Wu, L.; Zhang, X.; Rossini, M.; Wu, Y.; Zhang, Z.; Zhang, Y. Physiological dynamics dominate the response of canopy far-red solar-induced fluorescence to herbicide treatment. *Agric. For. Meteorol.* **2022**, *323*, 109063. [[CrossRef](#)]
82. He, L.; Magney, T.; Dutta, D.; Yin, Y.; Köhler, P.; Grossmann, K.; Stutz, J.; Dold, C.; Hatfield, J.; Guan, K. From the ground to space: Using solar-induced chlorophyll fluorescence to estimate crop productivity. *Geophys. Res. Lett.* **2020**, *47*, e2020GL087474. [[CrossRef](#)]
83. Cogliati, S.; Rossini, M.; Julitta, T.; Meroni, M.; Schickling, A.; Burkart, A.; Pinto, F.; Rascher, U.; Colombo, R. Continuous and long-term measurements of reflectance and sun-induced chlorophyll fluorescence by using novel automated field spectroscopy systems. *Remote Sens. Environ.* **2015**, *164*, 270–281. [[CrossRef](#)]
84. Rossini, M.; Nedbal, L.; Guanter, L.; Ač, A.; Alonso, L.; Burkart, A.; Cogliati, S.; Colombo, R.; Damm, A.; Drusch, M. Red and far red Sun-induced chlorophyll fluorescence as a measure of plant photosynthesis. *Geophys. Res. Lett.* **2015**, *42*, 1632–1639. [[CrossRef](#)]
85. Daumard, F.; Champagne, S.; Fournier, A.; Goulas, Y.; Ounis, A.; Hanocq, J.; Moya, I. A field platform for continuous measurement of canopy fluorescence. *IEEE Trans. Geosci. Remote Sens.* **2010**, *48*, 3358–3368. [[CrossRef](#)]
86. Millar, A.J.; Kay, S.A. Integration of circadian and phototransduction pathways in the network controlling CAB gene transcription in Arabidopsis. *Proc. Natl. Acad. Sci. USA* **1996**, *93*, 15491–15496. [[CrossRef](#)] [[PubMed](#)]
87. Muller, P.; Li, X.; Niyogi, K.K. Non-photochemical quenching. A response to excess light energy. *Plant Physiol.* **2001**, *125*, 1558–1566. [[CrossRef](#)] [[PubMed](#)]
88. Moya, I.; Loayza, H.; López, M.L.; Quiroz, R.; Ounis, A.; Goulas, Y. Canopy chlorophyll fluorescence applied to stress detection using an easy-to-build micro-lidar. *Photosynth. Res.* **2019**, *142*, 1–15. [[CrossRef](#)] [[PubMed](#)]
89. Loayza, H.; Moya, I.; Quiroz, R.; Ounis, A.; Goulas, Y. Active and passive chlorophyll fluorescence measurements at canopy level on potato crops. Evidence of similitude of diurnal cycles of apparent fluorescence yields. *Photosynth. Res.* **2023**, *155*, 271–288. [[CrossRef](#)] [[PubMed](#)]
90. Tao, F.; Zhang, L.; Zhang, Z.; Chen, Y. Climate warming outweighed agricultural managements in affecting wheat phenology across China during 1981–2018. *Agric. For. Meteorol.* **2022**, *316*, 108865. [[CrossRef](#)]
91. Aghaee, A.; Moradi, F.; Zare-Maivan, H.; Zarinkamar, F.; Irandoost, H.P.; Sharifi, P. Physiological responses of two rice (*Oryza sativa* L.) genotypes to chilling stress at seedling stage. *Afr. J. Biotechnol.* **2011**, *10*, 7617–7621.
92. Dodd, A.N.; Salathia, N.; Hall, A.; Kévei, E.; Tóth, R.; Nagy, F.; Hibberd, J.M.; Millar, A.J.; Webb, A.A. Plant circadian clocks increase photosynthesis, growth, survival, and competitive advantage. *Science* **2005**, *309*, 630–633. [[CrossRef](#)]
93. Cheng, X.; Hu, M.; Zhou, Y.; Wang, F.; Liu, L.; Wang, Y.; Huang, H.; Zhang, J. The divergence of micrometeorology sensitivity leads to changes in GPP/SIF between cork oak and poplar. *Agric. For. Meteorol.* **2022**, *326*, 109189. [[CrossRef](#)]

Disclaimer/Publisher’s Note: The statements, opinions and data contained in all publications are solely those of the individual author(s) and contributor(s) and not of MDPI and/or the editor(s). MDPI and/or the editor(s) disclaim responsibility for any injury to people or property resulting from any ideas, methods, instructions or products referred to in the content.